Physics of Plasmas

Meter-scale plasma waveguides for multi-GeV laser wakefield acceleration

Cite as: Phys. Plasmas **29**, 073101 (2022); https://doi.org/10.1063/5.0097214
Submitted: 26 April 2022 • Accepted: 08 June 2022 • Published Online: 01 July 2022

J. E. Shrock, B. Miao, L. Feder, et al.

Physics of Plasmas ARTICLE scitation.org/journal/php

Meter-scale plasma waveguides for multi-GeV laser wakefield acceleration

Cite as: Phys. Plasmas **29**, 073101 (2022); doi: 10.1063/5.0097214
Submitted: 26 April 2022 · Accepted: 8 June 2022 ·
Published Online: 1 July 2022

View Online Export Citation CrossMark

J. E. Shrock, B. Miao,[a] L. Feder, and H. M. Milchberg[b]

AFFILIATIONS

Institute for Research in Electronics and Applied Physics and Department of Physics, University of Maryland, College Park, Maryland 20742, USA

Notes: Part of Papers from the 63rd Annual Meeting of the APS Division of Plasma Physics special collection.
Note: Paper CI1 1, Bull. Am. Phys. Soc. 66 (2021).
[a]Invited speaker.
[b]**Author to whom correspondence should be addressed:** milch@umd.edu

ABSTRACT

We present results from two new techniques for the generation of meter-scale, low density ($\sim 10^{17}$ cm^{-3} on axis) plasma waveguides, the "two-Bessel" technique, and the "self-waveguiding" technique. Plasma waveguides of this density and length range are needed for demonstration of a ~10 GeV laser wakefield accelerator module, key for future staging for a ~TeV lepton collider. Both techniques require the use of high quality ultrashort pulse Bessel beams to efficiently and uniformly ionize hydrogen gas in meter-scale supersonic gas jets via optical field ionization. We review these two techniques, describe our meter-scale gas jets, and present a new method for correction of optical aberrations in Bessel beams. Finally, we briefly present results from recent experiments employing one of our techniques, demonstrating quasi-monoenergetic acceleration of ~5 GeV electron bunches in 20 cm long, low density plasma waveguides.

I. INTRODUCTION

Conventional metal cavity-based charged particle accelerators are limited by RF breakdown to acceleration gradients of 100 MeV/m,[1] so the size and cost of multi-GeV devices are considerable.[2] Laser wakefield accelerators use ultra-intense laser pulses to drive plasma waves with accelerating gradients up to ~100 GeV/m, with several proof-of-principle experiments demonstrating multi-GeV electron acceleration[3–5] and pointing the way to future practical laser-driven accelerators of greatly reduced size and cost.[6] A key step in this development is the demonstration of a high repetition rate, ~10 GeV laser wakefield acceleration (LWFA) module. For a ~1 TeV-scale center of mass lepton collider, the sequential staging[7] of dozens of these modules is envisioned.[6]

For a given plasma density, the maximum energy gain through LWFA is limited by dephasing of electrons and depletion of the drive laser pulse energy. As an electron gains energy from acceleration in the plasma wake, after a characteristic distance L_d, its velocity exceeds the plasma wake phase velocity and it is decelerated. Depletion occurs as laser energy is coupled into the plasma wave. Accounting for these effects, the energy gain in a LWFA scales as

$$\Delta W/mc^2 \sim a_0^r N_{cr}/N_e, \quad (1)$$

where a_0 is the normalized vector potential [$a_0 \sim 9 \times 10^{-10} I^{1/2}$ (W/cm^2)$\lambda(\mu$m), where I is the peak laser intensity in W/cm^2 and λ is the wavelength in μm], $r = 2$ in the quasilinear regime ($a_0 >\sim 1$), and $r = 1$ in the 3D nonlinear blowout regime ($a_0 \gg 1$), N_{cr} is the critical density, and N_e is the plasma density.[1] The expression for $\Delta W/mc^2$ shows that achieving multi-GeV electron bunches with LWFA requires both sufficiently low plasma density N_e and high laser intensity ($\propto a_0^2$) to drive a relativistic plasma wake over a distance $\sim L_d$. This is typically many Rayleigh ranges $z_0 = \pi w_0^2/\lambda$ of the focused laser pulse (w_0 is the laser spot size $1/e^2$ intensity radius and λ is the wavelength), with diffractive transverse spreading normally decreasing the intensity by many orders of magnitude.

Diffraction can be countered by optical guiding, which can preserve the pulse intensity and mode quality over distances long compared to a Rayleigh range. Guiding of high-intensity pulses in plasma has been achieved through relativistic self-guiding,[8,9] a relativistic nonlinear effect requiring $a_0 \gg 1$, and in preformed plasma waveguides generated by lasers[10] or capillary discharges,[11,12] where guiding of $a_0 \ll 1$ through $a_0 \gg 1$ pulses is possible, with self-guiding dominating the preformed structure at high a_0. The advantages of laser-generated plasma waveguides [especially those

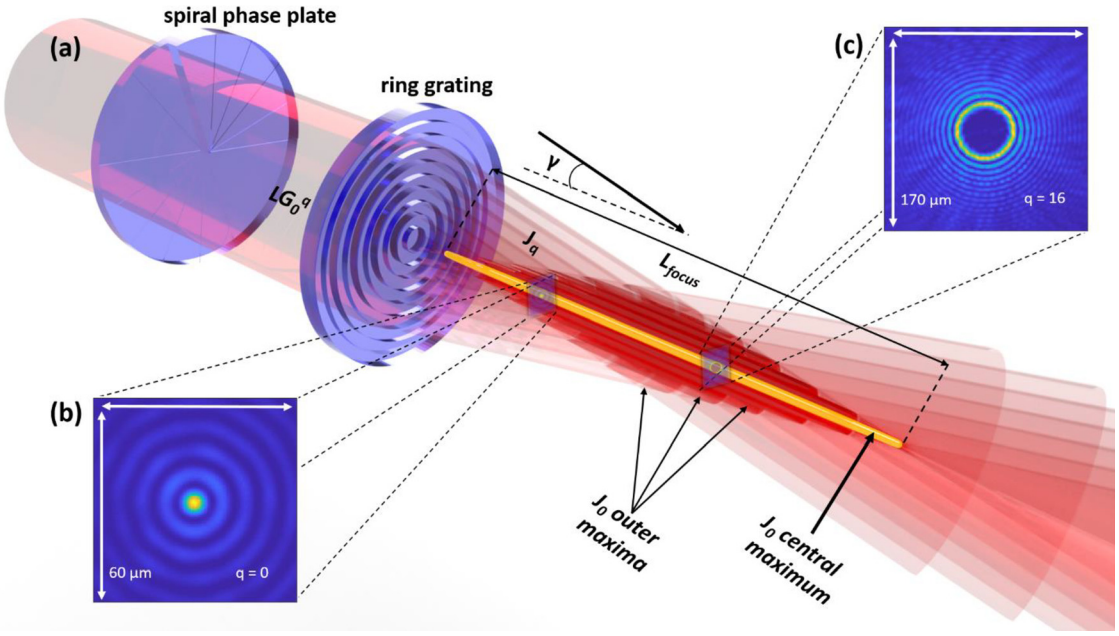

FIG. 1. Bessel beam formation. (a) Cutaway schematic of Bessel beam formation. A collimated, finite aperture beam passes through a spiral phase plate and ring grating to form a J_q Bessel beam. The radial phase applied by the ring grating causes each annulus of the incident beam to approach the transmission axis at an angle γ, generating the quasi-uniform, extended Bessel beam focus of length $L_{focus} \approx (R_b - a_h)/\tan\gamma$, where R_b is the beam radius and a_h is the radius of a central driver beam access hole in the ring grating (not shown). (b) and (c) Measured intensity profiles of J_0 and $J_{q=16}$ beams generated by this approach.

generated using gas jets (see Sec. III)] over capillary discharge waveguides are described in Sec. IV.

Multi-GeV acceleration[4,5] has been demonstrated using relativistic self-guiding in the blowout regime, but self-guiding at the low N_e needed for multi-GeV gain demands $a_0 \gg 1$ and at least petawatt (10^{15} W) laser power. The power required per GeV of acceleration is significantly reduced using preformed plasma waveguides, where a laser wakefield accelerator can be operated in the quasilinear regime ($a_0 \gtrsim 1$).[7] For laser intensity with $a_0 \gtrsim 1$, an electron energy gain of 10 GeV requires $N_e \sim 10^{17}$ cm^{-3}. This corresponds to a dephasing length, $L_d <\sim 1$ m, which sets the meter-scale length L_{guide} required for the plasma waveguide. Plasma waveguides also enable independent control of the guided laser mode structure and propagation characteristics, as well as control over dephasing, depletion, and phase matching in electron acceleration.[13–18]

Recently, we have developed two new approaches for the optical generation of meter-scale low density plasma waveguides suitable for multi-GeV laser wakefield acceleration in the quasilinear regime: the two-Bessel method[19] and the self-waveguiding[20] method. Both methods require generation and wavefront correction of Bessel beams.[21] We have subsequently implemented the self-waveguiding method in the first demonstration of multi-GeV laser wakefield acceleration in a fully optically formed plasma waveguide, achieving the highest recorded energies for electron bunches accelerated in an all-optical LWFA.[22] In this paper, we will review the key methods and diagnostics of our two plasma waveguide generation techniques and review our method for *in situ* wavefront correction of Bessel beams, which is crucial for their successful implementation.

II. BESSEL BEAMS

The use of Bessel beams is central to our generation of long, low density plasma waveguides. We use the symbol J_q to denote a physical Bessel beam of order q, whose experimental electric field profile near the optical axis closely follows the functional form of the qth order Bessel function, $E(r) \propto J_q(k_\perp r)$. Here, r is the radial distance from the optical axis and $k_\perp = k \sin\gamma$, where k is the laser wavenumber and γ is the axis approach angle for the rays forming the Bessel beam (see Fig. 1). While the mathematical Bessel function is of infinite transverse extent, an experimental Bessel beam is necessarily of finite aperture and, therefore, of finite axial extent.

Figure 1 shows how our J_q beams are generated. A finite aperture, parallel input beam of radius R_b propagating along z is incident on an optical element that imparts a linearly increasing azimuthal phase shift $\Delta\Phi_{azi}(r', \varphi') = q\varphi'$, followed by an element that imposes a radial phase shift $\Delta\Phi_{rad}(r', \varphi') = k(R_b - r')\tan\gamma$ for $r' < R_b$. Here, $(r', \varphi',$ and $z)$ are cylindrical coordinates at the location of the phase plates and (r, φ, z) are coordinates in the focal plane of the Bessel beam. In our experiments, the azimuthal phase shifting element is a qth order spiral phase plate[19] and the radial phase shifting element is either a reflective axicon[19,20] or a transmissive ring grating (or diffractive axicon)[22] [shown in Fig. 3(a)] with a central hole of radius a_h (not shown) to allow injection of a LWFA driver pulse into the waveguide. The spiral phase plates and ring gratings are designed based on Refs. 23 and 24 and fabricated by us at the University of Maryland using plasma etching on 0.5 mm thick or 1 mm thick fused silica wafers (for ring gratings and spiral phase plates, respectively). The spiral phase plates are discretized in 8 levels and the ring gratings in four levels. For generation of J_0 beams, the spiral phase plate is removed from the

beam path. The Bessel beam forms after the axicon, with the field profile nearly invariant over a distance $L_{focus} \approx (R_b - a_h)/\tan\gamma$, as shown by the ray construction in Fig. 1. Here, L_{focus} can be considered the depth of focus of the axicon or the length of the focal line. Generation of a plasma waveguide of length L_{guide} in a gas target (see below) requires that $L_{focus} > L_{guide}$ (see Sec. IV).

In applying Bessel beams to plasma waveguide generation, it is important that the highest intensity for a given pulse energy be generated in the central maximum of a J_0 beam, or uniformly around the first ring in a $J_{q>0}$ beam. This is equivalent to maximizing the fidelity of the near-axis portion of the beam to the Bessel functional form over the full length L_{focus}. In our experiments, the few-centimeter radius incident beam is both high energy and short pulse, making reflective axicons[19,20] and thin, transmissive ring gratings (diffractive axicons)[22] the best choice to avoid nonlinear phase distortion on the beam or optical damage. However, wavefront aberrations imparted by these optical elements (as well as those present in the incident beam) can significantly degrade the quality of the Bessel beam, with resulting poor fidelity to the Bessel functional form. While correction of wavefront aberration is a common procedure in optics, and real-time correction of aberrations in Gaussian beams has been well-studied,[25–27] these techniques are not readily applicable to the *in situ* wavefront correction of Bessel beams needed for plasma waveguide generation.

To solve this problem, we have developed a new technique to directly retrieve the complex amplitude of a Bessel beam from intensity measurements only.[21] In conjunction with a deformable mirror, this allows for reliable correction of standard Zernike aberrations[27] encountered in our use of axicons or ring gratings. For either of these elements, the radial phase profile imparted to the incident beam results in the mapping of each differential annulus of the incident beam to a point along the Bessel beam focal line. By resolving the measured field profile at a point along the focal line into a Bessel function basis and comparing with an ideal Bessel beam, we can find the phase aberrations in the corresponding azimuthal slice of the incident beam. By using images at different points along the focal line, we are able to generate a full phase map of the aberrations and correct them with a deformable mirror. The uncorrected and corrected J_0 beam focus along z is shown in Figs. 2(a)–2(e), and 2(a′)–2(e′). Note that for $z >$ 150 mm (farther from the axicon, toward the end of the focal line), the uncorrected focal intensity profile is substantially deteriorated from the desired form and would generate a highly asymmetric initial plasma. Deterioration of the focal profile is even more pronounced for high order Bessel beams, as shown in Figs. 2(f)–2(j), and 2(f)′–2(j′), for an uncorrected and corrected J_{16} beam. This correction technique was employed in the experiments described in Refs. 19, 20, and 22.

III. METER-SCALE GAS JET TARGETS

A suitable laser-generated plasma waveguide for a high-repetition rate, ∼10 GeV LWFA module requires a gas profile that is low density ($\sim 10^{17} - 10^{18}$ cm^{-3}) and long (up to tens of cm so that $L_{guide} \lesssim L_d$), with controllable longitudinal density variation (down to scales $\sim z_0$) and accessible for diagnostic measurements of the waveguide and the LWFA process.[28] While some of these criteria are met by gas cells,[29] the gas flow through the large-aperture laser access pinholes significantly limits the sharpness of the gas density ramps at the entrance and exit of the waveguide and limits the steady state density of the gas. Gas cells offer little control over longitudinal density variation, and their required laser access pinholes are susceptible to damage and widening by both the waveguide generating pulse (Bessel beam) and the guided LWFA driver pulse. The structural requirements of a gas cell can also limit diagnostic access to the waveguide and the LWFA process.

Using a gas jet, however, a free-standing plasma waveguide can be generated in the gas plume away from the jet nozzle, and the full length of the waveguide is accessible for diagnostics. When operated in the steady-state flow regime, the repetition rate is limited only by the available vacuum pumping speed (assuming a high repetition rate laser is available to generate the waveguide). The gas density ramps at the ends of the jet can be significantly sharpened by the supersonic flow, while the transverse gas density local profile is nearly uniform on the small transverse scales required for LWFA. We have implemented all of these features in the jets used in Refs. 19, 20, and 22. Though the specifics vary in each of these experiments, the general design was the same: high-pressure gas backs multiple solenoid valves and flows into a small reservoir beneath a narrow throat. The flow becomes supersonic as the gas moves into the wider region above the throat. We have developed jets up to 50 cm in length. For all of our experiments, we have used H_2 gas because it is fully ionized at the relatively low OFI threshold of $\sim 10^{14}$ W/cm^2.[30]

The longitudinal density profile of the extended hydrogen plume is characterized through a novel fluorescence measurement technique. An example of this technique applied to the jet used in Ref. 22 is shown in Figs. 3(a)–3(a″). A J_0 pulse is focused in the H_2 jet, generating a plasma column via OFI. The recombination fluorescence is imaged through a 656 nm bandpass filter, which restricts the measurement to the H-alpha line [Fig. 3(a)]. The abrupt ends in the

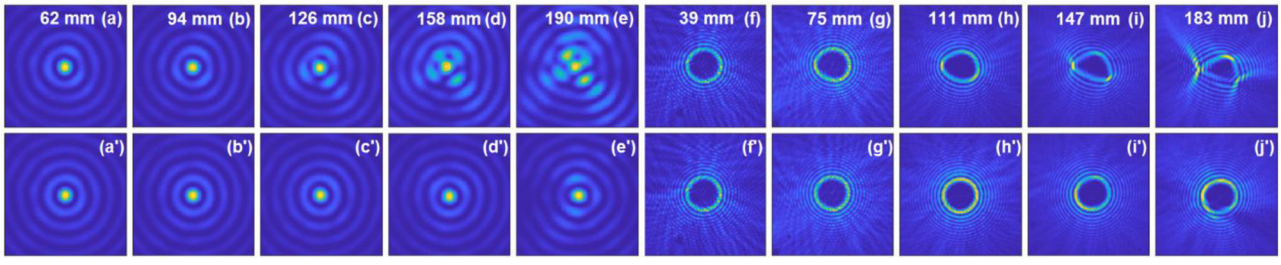

FIG. 2. Examples of corrected Bessel beams applied to plasma waveguide generation by OFI. (a)–(e) and (a′)–(e′) show the uncorrected and corrected intensity profiles for a J_0 Bessel beam formed with a reflective axicon at different points along the focal line. The window size is 59×59 μm^2. (f)–(j) and (f′)–(j′) show the same for a J_{16} beam. The window size is 168×168 μm^2.

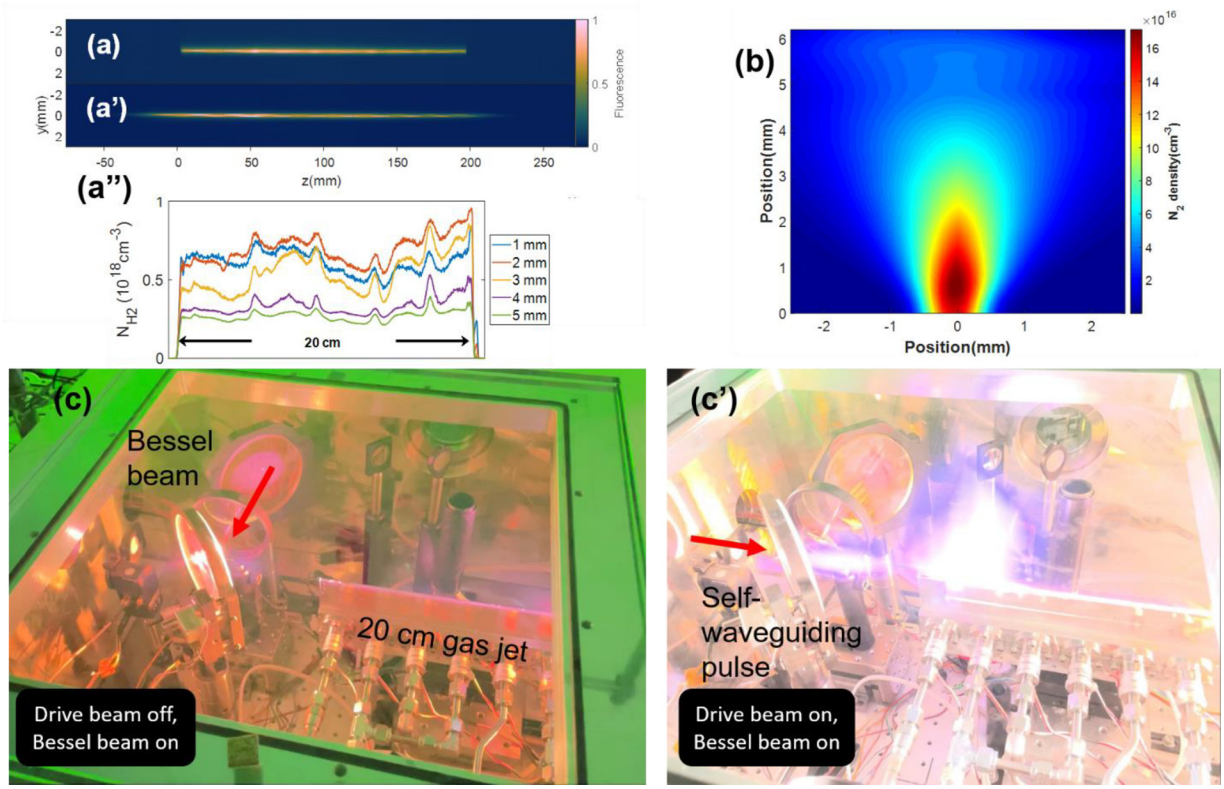

FIG. 3. Long, low density gas jets. (a) Sample fluorescence from optical field ionization of a 20 cm long H_2 gas jet by the J_0 pulse. (a′) Sample backfill fluorescence measurement with the jet in the same position as in (a) but with the valves off. (a′′) Extracted longitudinally resolved H_2 density profiles of a 20 cm long jet, at various heights above the jet. (b) Transverse density profile from longitudinal interferometry of the 20 cm jet used in Ref. 22. (c)–(c′) *In situ* photographs of the jet from the experiments in Ref. 22. Fluorescence from J_0-formed plasma is shown above the nozzle orifice in (c). In (c′), fluorescence is shown from self-waveguiding (see Sec. IV) of a 300 TW LWFA drive pulse.

fluorescence image of Fig. 3(a) are determined by the sharp ∼2 mm falloff in gas density at the ends of the jet. While the fluorescence intensity is proportional to the z-dependent H_2 density at that location, an absolute calibration of this measurement is still needed. This is accomplished by filling the experimental vacuum chamber with variable known pressures of hydrogen and generating OFI plasmas with the jet nozzle still in place but with the valves closed [see Fig. 3(a′)]. Since the gas now uniformly fills the region around the gas jet, any z-dependence in fluorescence intensity is caused by longitudinal variation in the J_0 beam profile over the focal length, L_{focus}. Therefore, in regions where the fluorescence above the pulsed jet does not have the same shape as the backfill fluorescence, the gas density is nonconstant. The gas density at a longitudinal position z is then found by interpolating the density as a function of backfill fluorescence intensity at the same z, and calculating the density corresponding to the measured jet fluorescence [Fig. 3(a′′)].

To date, the RMS longitudinal variation in our jets' density is $< 25\%$, due to various flaws in jet fabrication. This variation has had little impact on the waveguide mode structure since the plasma density difference between waveguide core and cladding is large, but it could have more significant effects on LWFA electron bunch quality, as discussed in Ref. 22. The longitudinally averaged transverse H_2 density profile is measured through shearing interferometry of a longitudinal probe pulse [Fig. 3(b)]. Figures 3(c)–3(c′) shows the jet *in situ* during the experiments in Ref. 22. Figure 3(c) shows fluorescence due to plasma generation by a J_0 pulse in the pulse gas sheet above the nozzle, and Fig. 3(c′) shows the significant additional fluorescence from self-waveguiding (see Sec. IV) of a ∼300 TW injected laser pulse.

IV. METER-SCALE, LOW DENSITY PLASMA WAVEGUIDES

Long plasma waveguides are essential to reach dephasing-limited acceleration ($L_{guide} > L_d$) in laser wakefield accelerators in the quasilinear regime. Both the waveguide's on-axis plasma density N_{e0} and the $1/e^2$ intensity radius w_{ch} of the guided drive laser pulse determine the acceleration energy gain for a given peak laser power, as determined using Eq. (1). For multi-GeV gain, L_{guide} can be hundreds of Raleigh ranges z_0 in extent,[19] where λ is the central wavelength of the drive laser.

The first demonstration of a plasma waveguide for high intensity laser pulses[10] used a 100 ps duration J_0 Bessel beam to ionize and heat a gas target to plasma densities $\sim 10^{19}$ cm^{-3} and temperatures ∼100 eV. The long pulse duration and high density promoted inverse Bremsstrahlung (IB) plasma heating. The ionization and heating was primarily driven by the high intensity central maximum of the J_0 beam, of radius $r = 2.405/k_\perp \approx 1\ \mu$m for the $\gamma = 25°$ refractive glass axicon used. For a beam of radius R_b incident on the axicon, and

axicon inner hole radius a_h (to allow injection of a driver pulse into the waveguide), the J_0 beam focus extended a distance $L_{focus} \approx (R_b - a_h)/\tan\gamma \sim 1$ cm, to form ~1 cm long, hot, narrow plasma column that drove a cylindrical blast wave[31] in the surrounding gas as it expanded, forming the radially increasing plasma density profile needed for a plasma waveguide structure. In close analogy to a traditional graded index optical fiber,[32] the radially increasing plasma density profile corresponds to a radially decreasing refractive index, owing to the dependence of the plasma refractive index, $n(r) \approx 1 - N_e(r)/2N_{cr}$, on plasma density N_e (N_{cr} is the critical density). Extending the analogy to a step-index fiber, the central region of the plasma acts as the waveguide "core" region and the shock region performs the function of the "cladding."

For plasma waveguides in the density range of interest for multi-GeV acceleration ($\sim 10^{17}$ cm^{-3}), IB heating is orders of magnitude less efficient, as its rate is proportional to N_e. Optical field ionization (OFI)[30] with femtosecond laser pulses has been explored as a method for hydrodynamic plasma waveguide formation[19,20,29,33–38] due to the fact that ionization of the working gas depends only on laser intensity and not on local gas density (Ref. 38 has recently demonstrated ~1 GeV electron acceleration using OFI-induced hydrodynamic plasma waveguides). OFI also significantly reduces the laser energy requirement compared to IB to reach fully ionized hydrogen, for example. The catch is that electron temperature $k_B T_e$ in the OFI process is limited to approximately the ponderomotive energy U_p in the laser field at the ionization threshold of the gas, $k_B T_e(\text{eV}) \sim U_p = 9.3\, I\,(10^{14}\,\text{W/cm}^2)\lambda(\mu\text{m})^2$. For hydrogen, the ionization threshold intensity is $I \sim 10^{14}$ W/cm^2 and $\lambda = 0.8\,\mu$m for the Ti:Sapphire lasers typically used, giving $k_B T_e \sim 10$ eV, an order of magnitude lower than in the IB case. This results in an insufficient pressure gradient to drive the radial shocks needed to form a strongly confining waveguide with a sufficiently thick cladding.[19,20]

An alternative approach for generating plasma waveguides, the capillary discharge,[11,12] has been used successfully in LWFA experiments. The plasma is formed by electric discharge and resistive heating along the axis of a long hydrogen-filled dielectric tube, typically formed from ceramic or sapphire. In the quasi-steady phase of the discharge under plasma pressure equilibrium, the high temperature on the capillary axis and the lower temperature at the inner wall forms a plasma waveguide structure with low plasma density on axis and high density at the wall. Typical central waveguide densities are $N_{eo} >\sim 5 \times 10^{18}$ cm^{-3}. To further reduce N_{eo} to the $<10^{18}$ cm^{-3} range needed for multi-GeV LWFA, a nanosecond laser IB heater pulse has recently been injected into a 20 cm long capillary discharge guide.[3,39] Nonetheless, capillary discharge waveguides still present multiple limitations for the development of high repetition rate LWFA: (1) discharge-induced capillary erosion and laser damage, (2) lack of flexible control over the density and the transverse shape and size of plasma waveguides, limiting control over possible guided modes and, thereby, the LWFA process, and (3) lack of diagnostic access to the plasma waveguide structure and to the guiding and acceleration processes inside the capillary.

Our two laser-based methods bypass the main limitations of capillary discharge waveguides: (1) Solid material structures are eliminated from the vicinity of plasma waveguide generation, especially using our meter-scale supersonic gas jets,[19,20,22] eliminating plasma- and laser-induced damage and enabling high repetition rate operation, (2) OFI is used to generate the waveguide, a process that is density independent, and allows multiple laser pulses to separately "imprint" the waveguide core and cladding, and (3) the free standing waveguide structure enables unlimited diagnostic beam and imaging access to the full length of the plasma waveguide.

In both waveguide generation methods, the waveguide core is generated by a J_0 pulse sufficiently intense (>10^{14} W/cm^2 in the central peak) to generate a plasma column via OFI. Although an OFI-generated plasma column is not hot enough to generate a cylindrical plasma shock of sufficient amplitude to serve as a low loss plasma cladding (which had led to very weak guided laser confinement, with leakage attenuation lengths ~1 cm[19,20,29,35,37]), as it expands it drives a cylindrical shock in the neutral gas at the plasma periphery. As this expansion proceeds, the on-axis plasma density drops by up to ~10×, with N_{e0} decreasing well below the initial hydrogen atom density. We call this low density plasma core surrounded by a higher-density neutral gas the "prepared index structure." Our two methods discussed below differ by how the neutral gas is ionized to form the cladding. Figure 4(a) plots the evolving plasma and neutral density profiles as a function of delay after a 75 fs FWHM J_0 pulse with mean intensity ~4.9×10^{15} W/cm^2 in the central maximum. The general form of the refractive index structure is well predicted by simulations,[20] which show that the shell expands steadily at the local speed of sound, $c_s = (\gamma_s k_B T_g/m)^{1/2} \sim 7 \times 10^5$ cm/s, where $\gamma_s = c_p/c_v$ is the ratio of specific heats, T_g is the hydrogen gas temperature (elevated by conduction from the adjacent few eV plasma), and m is the H_2 molecular mass. The plasma and neutral expansion and electron temperature are plotted in Fig. 4(b). Delaying the ionization of the outward propagating shell increases the waveguide core radius while minimally affecting the difference between core and cladding plasma densities, enabling control of the guided mode size.

The dashed curves in Fig. 4(a) and sample transverse interferometry in Fig. 4(c) and Fig. 4(c′) show that electron density expands from a peaked profile to a rather flat profile surrounded by a sharply rising neutral density shell. Once subsequent ionization of the neutral gas occurs, the overall plasma structure has a refractive index profile reminiscent of a step index optical fiber, as seen in Fig. 5. For a step-index fiber, the fundamental mode radius is $w_{ch} \approx a(0.6484 + 1.619V^{-3/2} + 2.879V^{-6} + , \ldots,)$, where a is the core radius, k is the laser wavenumber, and $V = ka(n_{core}^2 - n_{cladding}^2)^{1/2}$ is the step index fiber parameter.[40] For a plasma waveguide approximated as a step index fiber, $V = a(4\pi r_e \Delta N_e)^{1/2}$, where r_e is the classical electron radius and $\Delta N_e = N_e^{cladding} - N_e^{core}$ is the difference between the cladding and core plasma densities.[19]

A. The two-Bessel method

In the two-Bessel method, the neutral gas outside the plasma core undergoes OFI by a time-delayed higher order $J_{q>0}$ Bessel beam pulse whose maximum intensity ring overlaps the expanding neutral shell for a given delay. In effect, the J_q pulse imprints the plasma cladding around the core, producing a fully ionized plasma waveguide in hydrogen. For a fixed Bessel approach angle γ, a larger radius ring requires increased Bessel order q, or for fixed Bessel order q, a smaller γ will give a larger ring. In general, for small γ and $q > 1$, the radial position $r_{q,peak}$ of the intensity maximum of a J_q beam is given by $kr_{q,peak}\sin\gamma \approx 1.03q + 1.44$.[20] Figure 5 shows varying w_{ch} obtained by changing $r_{q,peak}$. The choice of hydrogen gas density in the jet, the

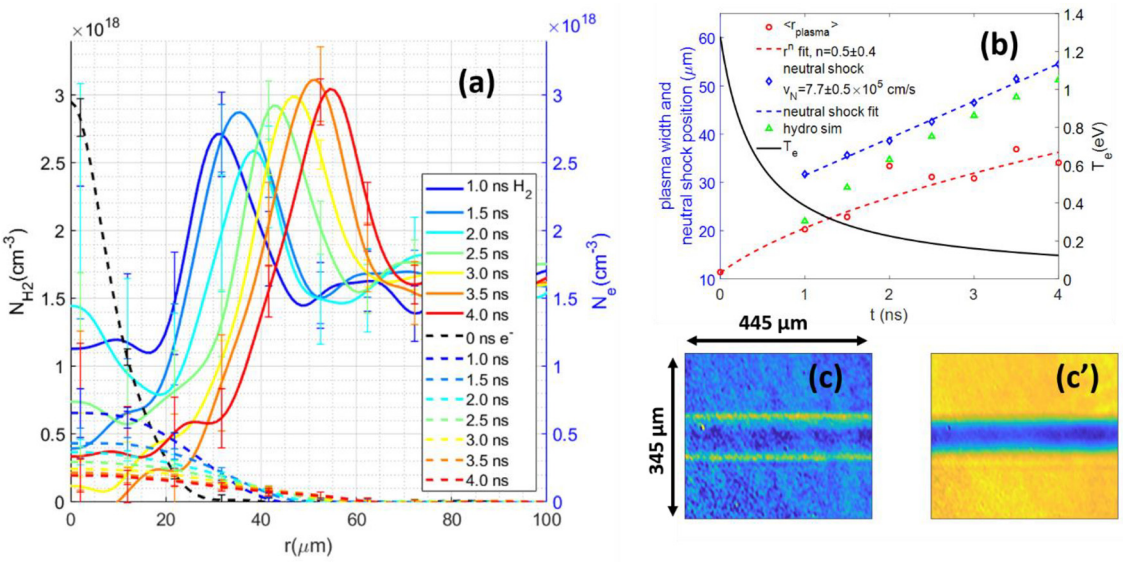

FIG. 4. (a) Hydrogen plasma and neutral gas profiles measured by two color interferometry[20] as a function of delay after on-axis plasma generation by a 75 fs FWHM 100 mJ pulse with a mean intensity 4.9×10^{15} W/cm^2 in the central maximum. The expansion of the neutral shell is nearly constant at $v_N \sim 7.7 \times 10^5$ cm/s. The neutral gas density profiles at different delays are plotted as solid lines (left axis scale), while the electron density profiles are plotted as dashed lines (right axis scale). (b) J_0 -induced rms plasma column radius (red circles) and neutral shock position (blue diamonds) with r^n plasma expansion fit (red dashed line) and constant $v_N \sim 7.7 \times 10^5$ cm/s neutral expansion fit (blue dashed line). Calculated electron temperature (black line) and shock expansion (green triangles) from hydrodynamic simulation are also shown. (c)–(c′) Sample results from two-color interferometry of "refractive index structure" induced by J_0 pulse. (c) Phase shift profile of neutral hydrogen, showing neutral shock at outside. (c′) Phase shift profile showing accompanying central plasma column.

values of axis approach angle γ and high order Bessel order q, and the post-J_0 delay of the J_q pulse are all "knobs" for controlling the guided mode size w_{ch} and group velocity v_g of the LWFA driver pulse.

B. The self-waveguiding method

The self-waveguiding method relies on the drive pulse itself to ionize the neutral shell.[20] For a sufficiently intense pulse injected end-on into the refractive index structure, the radial wings of the pulse's leading edge field-ionize the neutral shell, generating the waveguide cladding for the remainder of the pulse. In effect, the drive pulse generates its own plasma cladding on the fly, as seen in Fig. 6(a), which shows a snapshot from a particle-in-cell (PIC) simulation[41] of a weakly relativistic pulse self-waveguiding through a prepared index structure in hydrogen. Here, the injected 40 fs pulse has peak $a_0 = 0.3$ (peak intensity 1.9×10^{17} W/cm^2), and its spot size is chosen to match the lowest order mode size of the self-waveguiding-generated plasma waveguide.

In practice, w_{ch} can be selected to match w_0 by adjusting the delay between the J_0 pulse and the self-waveguiding pulse injected into the refractive index structure. An example of the effect of $w_0 \neq w_{ch}$ on self-waveguiding is shown in Fig. 6(b), which plots peak intensity vs propagation distance for three mode sizes with $a_0 = 0.37$ injected into a waveguide with $w_{ch} = 20\,\mu$m. Here, the simulation code used is YAPPE,[20] based on the unidirectional pulse propagation algorithm,[42] which gives good physical insight into propagation for $a_0 < 1$, where there is negligible plasma wave excitation. The intensity oscillations for the non-matched injected beams are caused by beating of the lowest order and first order radial modes,[13,20] an effect directly measured by imaging periodic intensity variations in plasma fluorescence after transmission of the self-waveguiding pulse. Figure 6(e) shows an example of these oscillations from self-waveguiding of an 88 mJ pulse over a 10 cm long prepared index structure. In Ref. 20, the measured frequency of 2.3 cm^{-1} is shown to agree with the mode-beating frequency predicted in Ref. 13. Under these conditions, the first-order mode leaks out of the guide, and the oscillations decay as the self-waveguiding pulse evolves into the fundamental mode of the waveguide. For higher intensity pulses, and higher density waveguides, $L_{1/e}$ for higher order modes can be longer than L_{guide}, resulting in multimode transmission through the guide (see Sec. V).

In Fig. 6(b), the energy decay is caused by leading edge erosion due to energy loss at the front of the pulse from diffraction, transverse leakage, and ionization. This loss is minimal for a high-energy LWFA drive pulse,[20,22] where $a_0 > 1$. For the $a_0 \sim 2.5$ pulse used in Ref. 22, the intensity exceeded the 10^{14} W/cm^2 hydrogen ionization threshold at the neutral shell position $r = 30\,\mu$m, 100 fs before the peak of the pulse. The minimal self-waveguiding energy cost for a high-intensity LWFA drive pulse is illustrated by the YAPPE simulation curve in Fig. 6(b) for a mode-matched pulse with $a_0 = 2$ and $w_0 = 20\,\mu$m, showing almost 100% transmission, neglecting damping from plasma wave generation to highlight self-waveguiding erosion alone. In practice, for the ~10 J pulses recently used in multi-GeV LWFA experiments,[22] we estimate that the small fraction of ~140 mJ was lost in far leading edge erosion from self-waveguiding. In LWFA experiments, however, the dominant guided pulse damping effect is plasma wave excitation; we have measured and simulated up to ~90% of the laser energy directed into this channel.[22]

Figure 6(c) shows that injection of pulses $w_0 \neq w_{ch}$ into the prepared index structure has little effect on the plasma waveguide

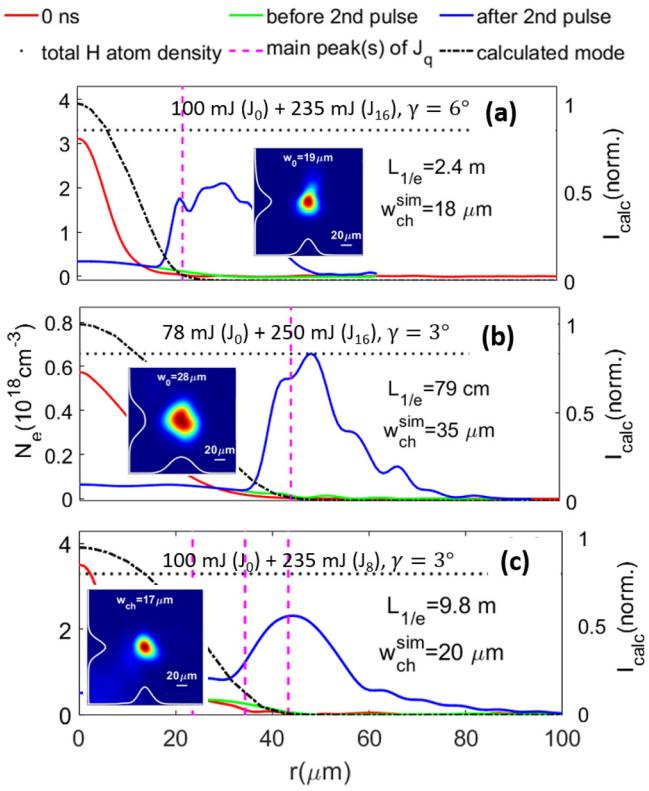

FIG. 5. Plasma density profiles and guided modes from the two-Bessel method. (a)–(c) Measured density profiles generated using q^{th} order Bessel beams with varying position $r_{q,peak}$ of the maximum intensity ring, obtained by varying q and approach angle γ. The solid blue curves plot the density profiles after ionization of the neutral shell by the J_q pulse. The red and green curves plot the initial plasma column formed by the J_0 pulse and the expanded plasma column immediately before passage of the J_q. The dashed pink line corresponds to the location of the first J_q maximum. The dash-dot black curve and w_{ch}^{sim} represent the calculated fundamental mode of the given plasma density profile,[13] and $L_{1/e}$ is the calculated $1/e$ attenuation length of the guided mode. The dotted line denotes the background atomic density of the neutral gas. The insets in each panel are representative guided modes measured after propagation in (a) 15, (b) 30, and (c) 30 cm guides at the given conditions.

generated once the mode-beating oscillations shown in Fig. 3(b) damp out. The necessary and sufficient feature of a prepared index structure to guarantee self-waveguiding are illustrated by Fig. 6(d): an on-axis neutral density minimum. Remarkably, neither a plasma core nor a neutral shock wall is necessary.

Measured density profiles of plasma waveguides generated by self-waveguiding pulses are plotted in Fig. 7. Here, the injected pulse energy ranges over 11–88 mJ, the initial hydrogen density over $1.3 - 2.8 \times 10^{18}$ cm^{-3}, and injection delay $\Delta\tau_{inj} = 1$–5 ns. Figure 7(a) highlights the effect of varying injected pulse energy on a fixed refractive index structure. At low injected pulse energy (11 mJ) only part of the neutral shock region is ionized. As injected energy increases, the plasma density profile becomes fully ionized and converges to the underlying ion (proton) density profile. The effect of varying the initial H_2 density is seen in Fig. 7(b), which shows that the radial position of the self-waveguiding-generated electron density peak is unchanged owing to the density independent expansion speed $c_s = (\gamma_s k_B T_g/m)^{1/2}$ of the neutral shell. Figure 7(c) shows that the waveguide structure can be modified to accommodate different mode sizes w_{ch} by varying the delay between the J_0 pulse and the self-waveguiding pulse. This allows for nearly independent tuning of the on-axis plasma density and guided mode size. We note that ionization by the wings of a guided pulse has been observed in a high density, several-millimeter long guide.[43] Early guiding results for OFI-heated plasma waveguides,[29,35] which otherwise would have been quite leaky,[19,20] have been more recently explained by self-waveguiding.[44]

While both the two-Bessel and self-waveguiding techniques are attractive for generating highly confining, low density guides with attenuation lengths extending to several meters and several hundred Rayleigh ranges,[19,20] their different cladding formation mechanisms result in different laser energy costs per unit length of waveguide. Detailed comparisons for the two methods suggest that self-waveguiding may be more efficient for experiments requiring smaller guided mode sizes, while the two-Bessel method is more efficient for larger mode sizes.[20]

For a longitudinally uniform H_2 jet density profile and sufficient pulse energy either in the J_0 and J_q beams of the two-Bessel method, or in the J_0 pulse and the self-waveguiding pulse, the resulting plasma waveguide will be axially uniform. Since full ionization of hydrogen occurs at a modest OFI intensity threshold $>10^{14}$ W/cm^2, relatively small energies of 1–2 J/m of waveguide are needed.[19,20] The main difference between two-Bessel- and self-waveguiding-generated guides are in the details of the transverse density profile, especially for wider waveguides.[20] Because the OFI yield per atom is independent of gas density, the main factor controlling the longitudinal density profile of the waveguide is the longitudinal H_2 jet density profile, which can be finely controlled with gas jet design. This is one of the advantages of gas jets over gas cells[37] or capillary discharges.[3]

V. APPLICATION TO MULTI-GEV ELECTRON ACCELERATION

Very recently, the self-waveguiding technique has been implemented in the first demonstration of LWFA generation of multi-GeV electron bunches in a fully optically formed plasma waveguide. These experiments took place on the ALEPH system at Colorado State University.[45] A drive pulse ($\lambda = 800$ nm, $\tau = 45$ fs, energy <15 J) self-waveguided over a 20 cm nitrogen doped hydrogen jet (5/95% mix, waveguide on-axis plasma densities $1.3 - 3.2 \times 10^{17}$ cm^{-3}), and accelerated electron bunches with quasi-monoenergetic peaks above 5 GeV and ~10 pC charge. An in-depth discussion of the experiment and results can be found in Ref. 22. Figure 8 gives an example of 8 of the highest energy spectra out of the hundreds of high energy spectra recorded.

The range of waveguide densities and drive pulse energies also enabled investigation of the self-waveguiding for pulses with $a_0 > 1$. Figures 9(a)–9(h) show characteristic waveguide exit modes after 20 cm under varying experimental conditions; Fig. 8(i) shows the injected mode on a larger scale. The transmission from monomode to multimode guiding occurs with increases in injected pulse energy, waveguide density, or Bessel beam energy. The first two quantities lead to more tightly confining guides: increased drive pulse energy enables more complete ionization of the neutral shell and surrounding background neutrals, while increased waveguide density corresponds to a higher background gas density and a greater difference between core

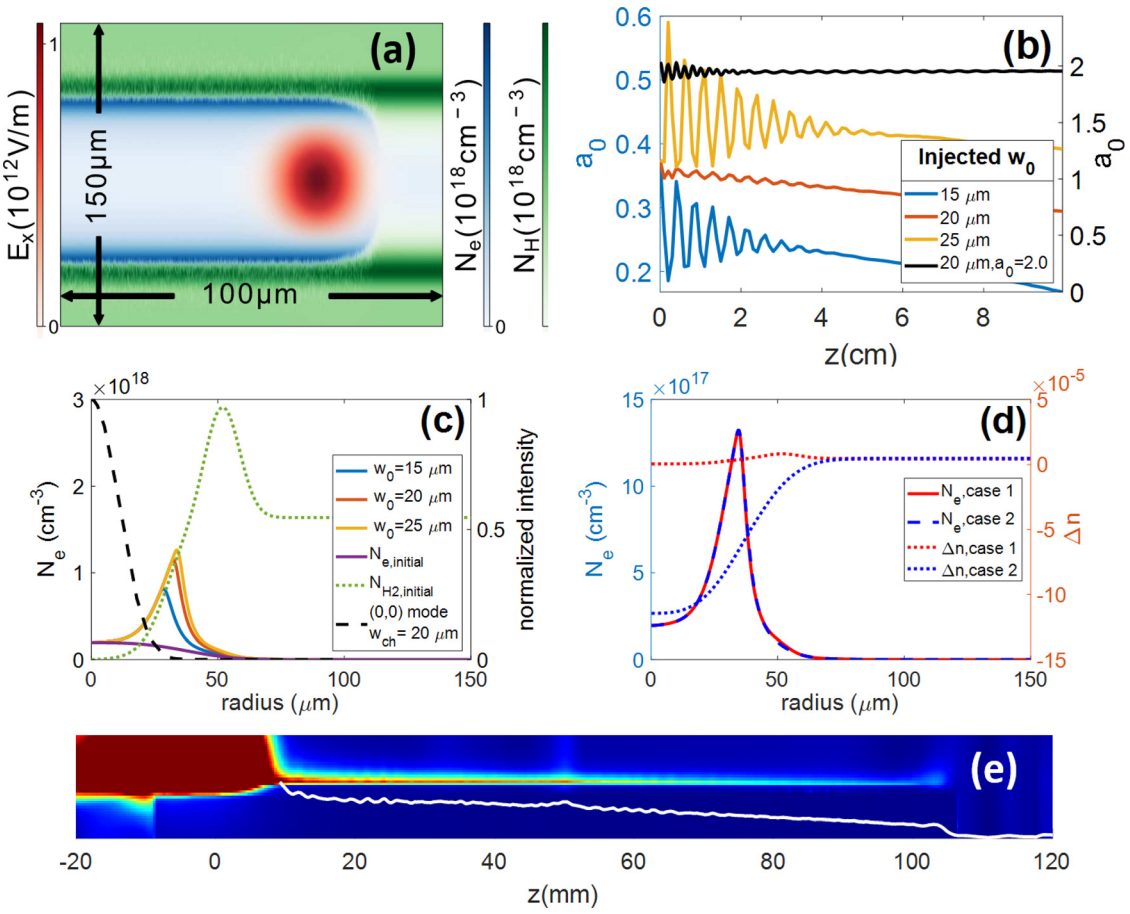

FIG. 6. Self-waveguiding in prepared index structures. (a) Particle-in-cell simulation of the self-waveguiding process in hydrogen using the quasi-cylindrical code FBPIC[41] for pulse width 40 fs, $a_0 = 0.3$. (b)–(d) Propagation simulations ($a_0 = 0.37$) using the code YAPPE,[20] illustrating (b) the effects of injection mode mismatch on the on-axis peak intensity as well as minimal energy loss from the self-waveguiding process for high intensity ($a_0 = 2$) pulses, (c) the minimal effect (at $z = 2$ cm) of mode mismatch on the downstream plasma waveguide transverse profiles after self-waveguiding, and (d) the necessary features of the prepared index structure to ensure self-waveguiding. (e) Imaged fluorescence profile after transmission of 88 mJ self-waveguiding pulse over 10 cm long prepared index structure, showing periodic fluorescence oscillations (column integration indicated by the white line) due to mode beating of the two lowest order guided modes. The laser is injected from the left and attenuates from self-waveguiding erosion as it propagates to the right.

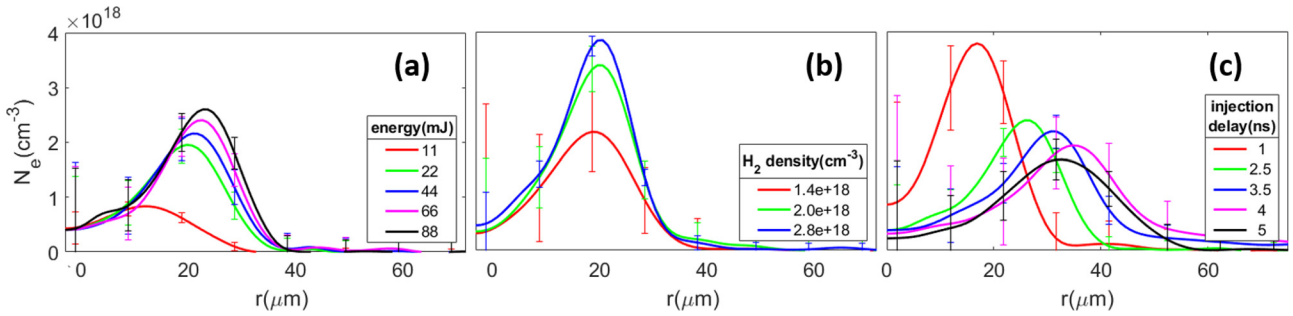

FIG. 7. Transverse interferometry of plasma profiles generated by self-waveguiding at z = 2 cm from entrance generated by self-waveguiding pulses (a) of different energies injected $\Delta\tau_{inj} = 2.5$ ns after the j_0 index-structuring pulse with $N_{H2} = 1.6 \times 10^{18}$ cm^{-3} initial hydrogen density (b) of 88 mJ injected at $\Delta\tau_{inj} = 2.5$ ns into prepared index structure with different initial hydrogen densities (c) of 88 mJ injected with varied $\Delta\tau_{inj}$ intro a prepared index structure with initial $N_{H2} = 1.6 \times 10^{18}$ cm^{-3}.

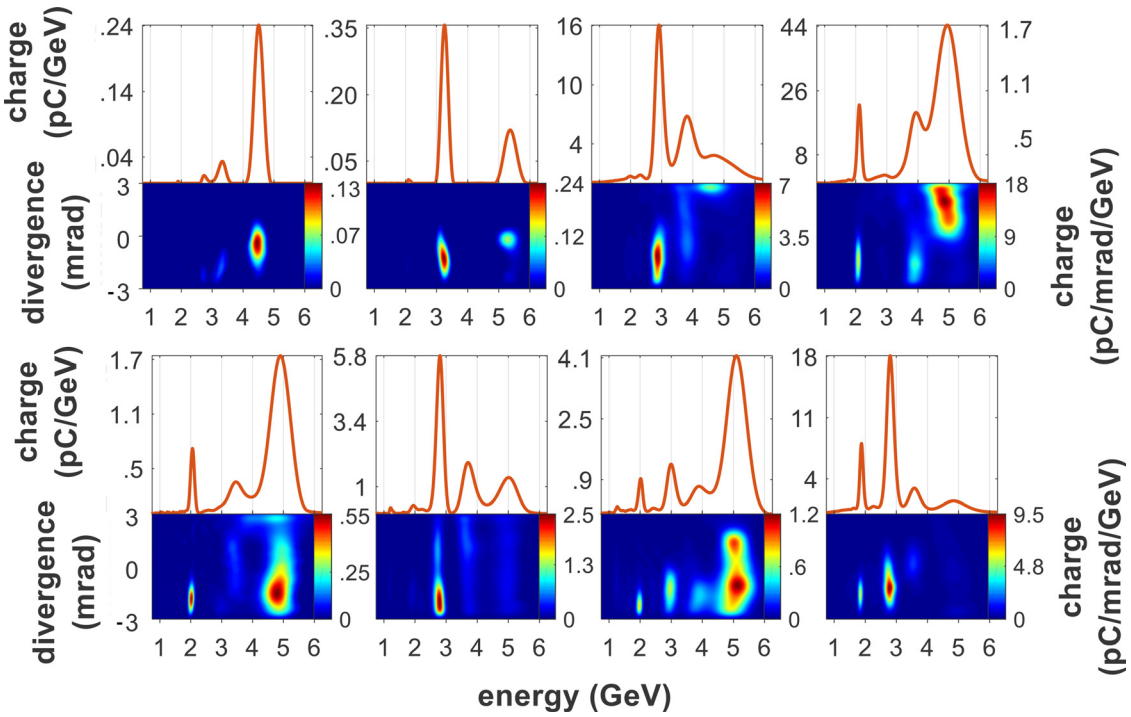

FIG. 8. Angle resolved spectra and lineouts for shots with the highest energy gain in Ref. 22. For all shots, the LWFA drive pulse energy was 11 J. The first two spectra had on-axis plasma density $N_{e0} = 1.3 \times 10^{17}$ cm^{-3} while the others had on-axis plasma density $N_{e0} = 1.6 \times 10^{17}$ cm^{-3}.

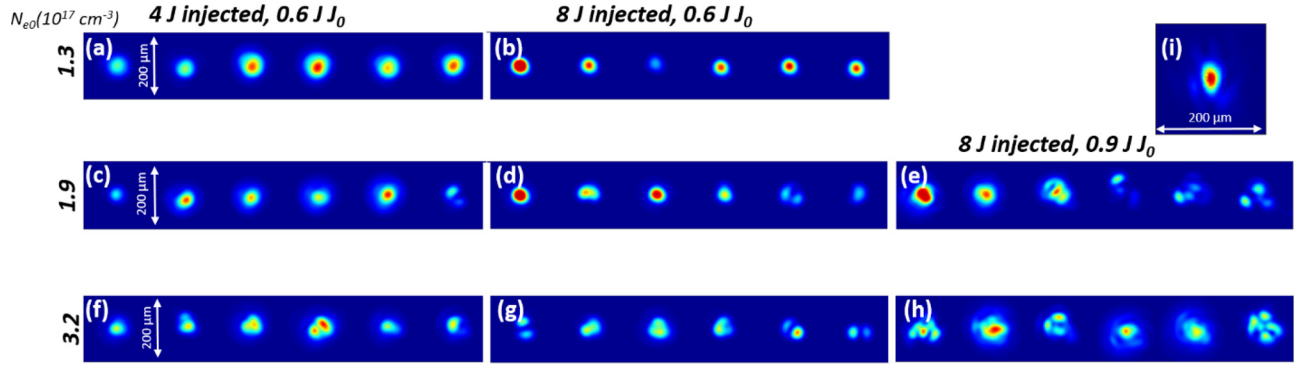

FIG. 9. (a)–(h) Guided modes for varying laser and plasma conditions, showing the transition from monomode to multimode guiding. All images were taken at the exit of a 20 cm waveguide, formed by self-waveguiding in prepared index structures in pure hydrogen. Although the self-waveguiding pulse was intense enough to excite plasma waves in the guide, there was no electron injection source for these measurements, such as the N_2 ionization injection source demonstrated in Ref. 22. All exit modes are plotted on the same spatial and intensity scales. (i) $f/25$ focal spot of injected drive pulse.

and cladding density. The tighter confinement means that higher order modes decay over $L_{1/e} > L_{guide} = 20$ cm and survive to the waveguide exit.[22] Though the waveguide fundamental mode size w_{ch} is matched to the injected pulse, slight variations in alignment between the drive pulse and the J_0 beam lead to coupling into these higher order modes. Increasing Bessel beam energy well beyond that required for OFI in the central maximum leads to ionization in the secondary rings of the Bessel beam, and a larger initial plasma column. As shown in Ref. 19, a larger diameter initial plasma column alters the expansion of the neutral shell, leading to a larger fundamental mode size. This means that the guide is no longer matched to the injected pulse, resulting in significant coupling into higher order modes [see panel (h)].

VI. CONCLUSION

Laser-wakefield acceleration (LWFA) of multi-GeV electron bunches in the quasilinear regime requires the implementation of plasma waveguides many times longer than the Rayleigh range of the drive pulse. Until recently, this had only been achieved with electric

discharge capillaries, leaving a need for an all-optical solution tailored for high repetition applications. We have demonstrated two new techniques for the all-optical generation of meter-scale plasma waveguides. These techniques independently form the waveguide core and cladding, allowing for the waveguide plasma and optical parameters to be carefully tuned for the desired LWFA drive pulse.

ACKNOWLEDGMENTS

The authors thank Elaine Taylor, Ela Rockafellow, Matthew Le, and Andrew Goffin (University of Maryland), and Reed Hollinger, John Morrison, Ryan Nedbailo, Huanyu Song, Shoujun Wang, and Jorge Rocca (Colorado State University) for technical discussions and assistance. High performance computing support to the University of Maryland was provided through the Office of Naval Research (No. N00014-20-1-2233). This work was supported by the U.S. Department of Energy (Nos. DE-SC0015516, LaserNetUS DE-SC0019076/FWP#SCW1668, and DE-SC0011375), and the National Science Foundation (Nos. PHY1619582 and PHY2010511).

AUTHOR DECLARATIONS

Conflict of Interest

The authors have no conflicts to disclose.

Author Contributions

J. E. Shrock: Conceptualization (equal); Data curation (equal); Formal analysis (equal); Investigation (equal); Methodology (equal); Software (equal); Validation (equal); Visualization (equal); Writing – original draft (equal); Writing – review and editing (equal). **B. Miao:** Conceptualization (equal); Data curation (equal); Formal analysis (equal); Investigation (equal); Methodology (equal); Software (equal); Supervision (equal); Validation (equal); Visualization (equal); Writing – review and editing (equal). **L. Feder:** Conceptualization (equal); Investigation (equal); Methodology (equal); Validation (equal); Visualization (equal); Writing – review and editing (equal). **H. M. Milchberg:** Conceptualization (equal); Data curation (equal); Formal analysis (equal); Funding acquisition (equal); Investigation (equal); Methodology (equal); Project administration (equal); Resources (equal); Software (equal); Supervision (equal); Validation (equal); Visualization (equal); Writing – original draft (equal); Writing – review and editing (equal).

DATA AVAILABILITY

The data that support the findings of this study are available from the corresponding author upon reasonable request.

REFERENCES

[1]E. Esarey, C. B. Schroeder, and W. P. Leemans, Rev. Mod. Phys. **81**, 1229 (2009).
[2]P. Emma, R. Akre, J. Arthur, R. Bionta, C. Bostedt, J. Bozek, A. Brachmann, P. Bucksbaum, R. Coffee, F. J. Decker, Y. Ding, D. Dowell, S. Edstrom, A. Fisher, J. Frisch, S. Gilevich, J. Hastings, G. Hays, P. Hering, Z. Huang, R. Iverson, H. Loos, M. Messerschmidt, A. Miahnahri, S. Moeller, H. D. Nuhn, G. Pile, D. Ratner, J. Rzepiela, D. Schultz, T. Smith, P. Stefan, H. Tompkins, J. Turner, J. Welch, W. White, J. Wu, G. Yocky, and J. Galayda, Nat. Photonics **4**, 641 (2010).
[3]A. J. Gonsalves, K. Nakamura, J. Daniels, C. Benedetti, C. Pieronek, T. C. H. de Raadt, S. Steinke, J. H. Bin, S. S. Bulanov, J. van Tilborg, C. G. R. Geddes, C. B. Schroeder, C. Tóth, E. Esarey, K. Swanson, L. Fan-Chiang, G. Bagdasarov, N. Bobrova, V. Gasilov, G. Korn, P. Sasorov, and W. P. Leemans, Phys. Rev. Lett. **122**, 084801 (2019).
[4]X. Wang, R. Zgadzaj, N. Fazel, Z. Li, S. A. Yi, X. Zhang, W. Henderson, Y. Y. Chang, R. Korzekwa, H. E. Tsai, C. H. Pai, H. Quevedo, G. Dyer, E. Gaul, M. Martinez, A. C. Bernstein, T. Borger, M. Spinks, M. Donovan, V. Khudik, G. Shvets, T. Ditmire, and M. C. Downer, Nat. Commun. **4**, 1988 (2013).
[5]H. T. Kim, K. H. Pae, H. J. Cha, I. J. Kim, T. J. Yu, J. H. Sung, S. K. Lee, T. M. Jeong, and J. Lee, Phys. Rev. Lett. **111**, 165002 (2013).
[6]C. B. Schroeder, E. Esarey, C. G. R. Geddes, C. Benedetti, and W. P. Leemans, Phys. Rev. Spec. Top. - Accel. Beams **13**, 101301 (2010).
[7]S. Steinke, J. Van Tilborg, C. Benedetti, C. G. R. Geddes, C. B. Schroeder, J. Daniels, K. K. Swanson, A. J. Gonsalves, K. Nakamura, N. H. Matlis, B. H. Shaw, E. Esarey, and W. P. Leemans, Nature **530**, 190 (2016).
[8]J. Osterhoff, A. Popp, Z. Major, B. Marx, T. P. Rowlands-Rees, M. Fuchs, M. Geissler, R. Hörlein, B. Hidding, S. Becker, E. A. Peralta, U. Schramm, F. Grüner, D. Habs, F. Krausz, S. M. Hooker, and S. Karsch, Phys. Rev. Lett. **101**, 085002 (2008).
[9]C. Joshi, IEEE Trans. Plasma Sci. **45**, 3134 (2017).
[10]C. G. Durfee and H. M. Milchberg, Phys. Rev. Lett. **71**, 2409 (1993).
[11]A. Butler, D. J. Spence, and S. M. Hooker, Phys. Rev. Lett. **89**, 185003 (2002).
[12]Y. Ehrlich, C. Cohen, A. Zigler, J. Krall, P. Sprangle, and E. Esarey, Phys. Rev. Lett. **77**, 4186 (1996).
[13]T. R. Clark and H. M. Milchberg, Phys. Rev. E **61**, 1954 (2000).
[14]P. Sprangle, B. Hafizi, J. R. Peñano, R. F. Hubbard, A. Ting, C. I. Moore, D. F. Gordon, A. Zigler, D. Kaganovich, and T. M. Antonsen, Phys. Rev. E **63**, 056405 (2001).
[15]B. D. Layer, A. York, T. M. Antonsen, S. Varma, Y.-H. Chen, Y. Leng, and H. M. Milchberg, Phys. Rev. Lett. **99**, 035001 (2007).
[16]C. Benedetti, C. B. Schroeder, E. Esarey, and W. P. Leemans, Phys. Plasmas **19**, 053101 (2012).
[17]S. J. Yoon, J. P. Palastro, and H. M. Milchberg, Phys. Rev. Lett. **112**, 134803 (2014).
[18]C. G. Durfee, J. Lynch, and H. M. Milchberg, Phys. Rev. E **51**, 2368 (1995).
[19]B. Miao, L. Feder, J. E. Shrock, A. Goffin, and H. M. Milchberg, Phys. Rev. Lett. **125**, 074801 (2020).
[20]L. Feder, B. Miao, J. E. Shrock, A. Goffin, and H. M. Milchberg, Phys. Rev. Res. **2**, 43173 (2020).
[21]B. Miao, L. Feder, J. E. Shrock, and H. M. Milchberg, Opt. Express **30**, 11360 (2022).
[22]B. Miao, J. E. Shrock, L. Feder, R. C. Hollinger, J. Morrison, R. Nedbailo, A. Picksley, H. Song, S. Wang, J. J. Rocca, and H. M. Milchberg, "Multi-GeV electron bunches from an all optical laser wakefield accelerator," available at arXiv:2112.03489.
[23]G. J. Swanson and W. B. Veldkamp, Opt. Eng. **28**, 286605 (1989).
[24]D. C. O'Shea, T. J. Suleski, A. D. Kathman, and D. W. Prather, *Diffractive Optics: Design, Fabrication, and Test* (SPIE Press, Bellingham, Washington, 2009).
[25]T. Čižmár, M. Mazilu, and K. Dholakia, Nat. Photonics **4**, 388 (2010).
[26]K. D. Wulff, D. G. Cole, R. L. Clark, R. DiLeonardo, J. Leach, J. Cooper, G. Gibson, and M. J. Padgett, Opt. Express **14**, 4170 (2006).
[27]J. Houzet, N. Faure, M. Larochette, A.-C. Brulez, S. Benayoun, and C. Mauclair, Opt. Express **24**, 6542 (2016).
[28]M. C. Downer, R. Zgadzaj, A. Debus, U. Schramm, and M. C. Kaluza, Rev. Mod. Phys. **90**, 35002 (2018).
[29]A. Picksley, A. Alejo, J. Cowley, N. Bourgeois, L. Corner, L. Feder, J. Holloway, H. Jones, J. Jonnerby, H. M. Milchberg, L. R. Reid, A. J. Ross, R. Walczak, and S. M. Hooker, Phys. Rev. Accel. Beams **23**, 081303 (2020).
[30]P. B. Corkum, N. H. Burnett, and F. Brunel, Phys. Rev. Lett. **62**, 1259 (1989).
[31]T. R. Clark and H. M. Milchberg, Phys. Rev. Lett. **78**, 2373 (1997).
[32]A. W. Snyder and J. D. Love, *Optical Waveguide Theory* (Chapman and Hall, London, 1984).
[33]N. Lemos, L. Cardoso, J. Geada, G. Figueira, F. Albert, and J. M. Dias, Sci. Rep. **8**, 3165 (2018).
[34]N. Lemos, T. Grismayer, L. Cardoso, G. Figueira, R. Issac, D. A. Jaroszynski, and J. M. Dias, Phys. Plasmas **20**, 063102 (2013).
[35]R. J. Shalloo, C. Arran, L. Corner, J. Holloway, J. Jonnerby, R. Walczak, H. M. Milchberg, and S. M. Hooker, Phys. Rev. E **97**, 053203 (2018).

[36]S. Smartsev, C. Caizergues, K. Oubrerie, J. Gautier, J.-P. Goddet, A. Tafzi, K. T. Phuoc, V. Malka, and C. Thaury, Opt. Lett. **44**, 3414 (2019).
[37]R. J. Shalloo, C. Arran, A. Picksley, A. von Boetticher, L. Corner, J. Holloway, G. Hine, J. Jonnerby, H. M. Milchberg, C. Thornton, R. Walczak, and S. M. Hooker, Phys. Rev. Accel. Beams **22**, 041302 (2019).
[38]K. Oubrerie, A. Leblanc, O. Kononenko, R. Lahaye, I. A. Andriyash, J. Gautier, J.-P. Goddet, L. Martelli, A. Tafzi, K. T. Phuoc, S. Smartsev, and C. Thaury, Light Sci. Appl. **11**, 180 (2022).
[39]N. A. Bobrova, P. V. Sasorov, C. Benedetti, S. S. Bulanov, C. G. R. Geddes, C. B. Schroeder, E. Esarey, and W. P. Leemans, Phys. Plasmas **20**, 020703 (2013).
[40]D. Marcuse, Bell Syst. Tech. J. **56**, 703 (1977).
[41]R. Lehe, M. Kirchen, I. A. Andriyash, B. B. Godfrey, and J.-L. Vay, Comput. Phys. Commun. **203**, 66 (2016).
[42]M. Kolesik and J. V. Moloney, Phys. Rev. E **70**, 036604 (2004).
[43]A. Morozov, A. Goltsov, Q. Chen, M. Scully, and S. Suckewer, Phys. Plasmas **25**, 053110 (2018).
[44]A. Picksley, A. Alejo, R. J. Shalloo, C. Arran, A. von Boetticher, L. Corner, J. A. Holloway, J. Jonnerby, O. Jakobsson, C. Thornton, R. Walczak, and S. M. Hooker, Phys. Rev. E **102**, 53201 (2020).
[45]Y. Wang, S. Wang, A. Rockwood, B. M. Luther, R. Hollinger, A. Curtis, C. Calvi, C. S. Menoni, and J. J. Rocca, Opt. Lett. **42**, 3828 (2017).